

Supplementary material

Aqueous SOA formation from the photo-oxidation of vanillin: Direct photosensitized reactions and nitrate-mediated reactions

Brix Raphael Go¹, Yan Lyu¹, Yan Ji¹, Dan Dan Huang², Xue Li³, Theodora Nah¹, Chun Ho Lam¹, and Chak K. Chan^{1*}

¹School of Energy and Environment, City University of Hong Kong, Hong Kong, China

²Shanghai Academy of Environmental Sciences, Shanghai 200233, China

³Institute of Mass Spectrometry and Atmospheric Environment, Jinan University No. 601 Huangpu Avenue West, Guangzhou 510632, China

Correspondence to: Chak K. Chan (Chak.K.Chan@cityu.edu.hk)

Text S1. Materials.

Initial solutions of 0.1 mM vanillin (VL, Acros Organics, 99%, pure), 0.1 mM guaiacol (GUA, Sigma Aldrich, $\geq 98.0\%$), 1 mM ammonium nitrate (AN, Acros Organics, 99+%, for analysis), 1 mM sodium nitrate (SN, Sigma-Aldrich, $\geq 99.5\%$), 1 mM of 2-propanol (IPA, Optima LC/MS grade), and 1 mM of sodium bicarbonate (NaBC, Fisher BioReagents, 99.7-100.3%) were prepared in Milli-Q water. The pH values of the samples were adjusted using sulfuric acid (H_2SO_4 ; Acros Organics, ACS reagent, 95% solution in water).

Text S2. UV-Vis spectrophotometric analyses.

The absorbance changes for all samples were characterized using a UV-Vis spectrophotometer (UV-3600, Shimadzu Corp., Japan). The absorbance values from 200 to 700 nm were recorded instantly after sample collection, and measurements were done in triplicate. Absorbance enhancements were calculated as the change in the integrated area of absorbance from 350 to 550 nm. The increase of light absorption at this wavelength range, where VL and GUA did not initially absorb light, suggests the formation of light-absorbing compounds (Zhou et al., 2019).

Text S3. UHPLC-PDA analyses.

An ultra-high performance liquid chromatography system (UHPLC, Waters Acquity H-Class, Waters, Milford, USA) coupled to a photodiode array (PDA) detector (Waters, Milford, USA) was used for the quantification of VL and GUA concentrations. The drawn solutions were first filtered through a 0.2 μm Chromafil[®]Xtra PTFE filter (Macherey-Nagel GmbH & Co. KG, Germany). Briefly, the separation of products was performed using an Acquity HSS T3 column (1.8 μm , 2.1 mm \times 100 mm; Waters Corp.). The column oven was held at 30 $^\circ\text{C}$, and the autosampler was cooled at 4 $^\circ\text{C}$. The injection volume was set to 5 μL . The binary mobile phase

consisted of A (water) and B (acetonitrile). The gradient elution was performed at a flow rate of 0.2 mL/min: 0-1 min, 10% eluent B; 1-25 min, linear increase to 90% eluent B; 25-29.9 min, hold 90% eluent B; 29.9-30 min, decrease to 10% eluent B; 30-35 min, re-equilibrate at 10% eluent B for 5 min. Standard solutions of VL and GUA ranging from 10 to 130 μ M were analyzed along with samples and blanks using the channels with UV absorption at 300 and 274 nm, respectively. The calibration curves for VL and GUA standard solutions are shown in Figure S2.

Text S4. IC analyses of small organic acids.

The small organic acids were analyzed using an ion chromatography system (IC, Dionex ICS-1100, Sunnyvale, CA) equipped with a Dionex AS-DV autosampler (Sunnyvale, CA). The separation was achieved using an IonPacTM AS15 column (4 \times 250 mm) with an AG15 guard column (4 \times 50 mm). The isocratic gradient was applied at a flow rate of 1.2 mL/min with 38 mM sodium hydroxide (NaOH) as the eluent. The total run time was set at 20 min. The standard solutions (1-50 μ M) of formic, succinic, and oxalic acid were analyzed three times along with the samples and water blank. Formic, succinic, and oxalic acid had retention times of 3.6 min, 8.3 min, and 11.9 min, respectively.

Text S5. UHPLC-qToF-MS analyses.

The characterization of reaction products was performed using a UHPLC system (ExionLCTM AD, ABSciex, Concord, Canada) coupled to a quadrupole time-of-flight mass spectrometer (qToF-MS) (TripleTOF 6600+, ABSciex). The settings (e.g., column, mobile phase, gradient, oven temperature) in the UHPLC system were the same as those used in UHPLC-PDA (Text S3). The mass spectrometer was equipped with an electrospray ionization (ESI) source and operated in the positive ion mode (the negative ion mode signals were too low for our analyses) at

a resolving power (full width at half-maximum (fwhm) at m/z 300) of 30000 in MS and 30000 in MS/MS (high-resolution mode). Information-dependent acquisition (IDA) scanning was adapted for product identification. The acquisition using IDA consisted of a ToF-MS scan and information-dependent trigger events. The ToF-MS scan had an accumulation time of 250 ms and covered a mass range of m/z 30-700 with a declustering potential (DP) of 40 and collision energy (CE) of 10 eV. The accumulation time for the IDA experiment was 100 ms, and the MS/MS scan range was set from m/z 30-700 in high-resolution mode. The IDA criteria were as follows: 5 most intense ions (number of IDA experiments) with an intensity threshold above 50 cps, isotope exclusion was switched off, and dynamic background subtraction was switched on. The automated calibration device system (CDS) was set to perform an external calibration every four samples. The ESI source conditions were as follows: temperature, 500 °C; curtain gas (CUR), 25 psi; ion source gas 1 at 50 psi; ion source gas 2 at 50 psi; and ion-spray voltage floating (ISVF) at 4.5 kV.

All parameters in the liquid chromatography system and mass spectrometer were controlled using Analyst TF Software 1.8 (ABSciex). The high-resolution LC-MS data were processed with PeakView and Analyst in the SCIEX OS software 1.5 (ABSciex). Peaks from the blank sample were subtracted from the sample signals. In addition to a minimum signal-to-noise ratio of 30, a peak was determined as a product if the difference in peak area between the samples before and after irradiation is ≥ 10 times. The formula assignments were carried out using the MIDAS molecular formula calculator (<http://magnet.fsu.edu/~midas/>) with the following constraints: $C \leq 35$, $H \leq 70$, $N \leq 5$, $O \leq 20$, $Na \leq 1$, and the mass error was initially set as 10 ppm. The nitrogen atom was removed in the constraints for the experiments without AN or SN. The detected adducts in ESI positive ion mode have several types (e.g., $[M+H]^+$, $[M+Na]^+$), and their formation can be influenced by the sample matrix (Erngren et al., 2019). For simplification purposes, we mainly

considered $[M+H]^+$ adducts for formula assignments, except for specific experiments with AN or SN in which $[M+NH_4]^+$ adducts and $[M+Na]^+$ adducts were observed. The final assigned formulas were constrained by a mass error mostly <5 ppm, which is a requirement for product identification using positive ion mode (Roemmelt et al., 2015). The double bond equivalent (DBE) values and carbon oxidation state (OS_c) of the neutral formulas were calculated using the following equations (Koch and Dittmar, 2006)

$$DBE = C - H/2 + N/2 + 1 \quad (\text{Eq. S1})$$

$$OS_c = 2 \times O/C - H/C \quad (\text{Eq. S2})$$

where C, H, O, and N correspond to the number of carbon, hydrogen, oxygen, and nitrogen atoms in the neutral formula, respectively. Based on the identified products, the average oxygen to carbon (O:C) ratios, $\langle O:C \rangle$: ($\langle O:C \rangle = \sum_i (\text{abundance}_i) O_i / \sum_i (\text{abundance}_i) C_i$) and average hydrogen to carbon (H:C) ratios, $\langle H:C \rangle$: ($\langle H:C \rangle = \sum_i (\text{abundance}_i) H_i / \sum_i (\text{abundance}_i) C_i$) after the reactions were further estimated using the signal-weighted method (Bateman et al., 2012). The average OS_c ($\langle OS_c \rangle$) was calculated as follows:

$$\langle OS_c \rangle = 2 \times \langle O:C \rangle - \langle H:C \rangle \quad (\text{Eq. S3})$$

Based on the typical MS/MS fragmentation behavior for individual functional groups (Table S1) and DBE values, examples of structures for products identified from VL (and GUA) photo-oxidation experiments were proposed (Table S3).

Text S6. Photon flux measurements.

In this work, 2-nitrobenzaldehyde (2NB), a chemical actinometer, was used to determine the photon flux in the aqueous photoreactor. We first measured the relative intensity of light passing through the empty reactor, then the reactor containing 50 μM 2NB using a high-sensitivity spectrophotometer (Brolight Technology Co. Ltd, Hangzhou, China) equipped with an optical fiber (Brolight). Then, the average relative intensity absorbed by 2NB solution as a function of wavelength was calculated. Briefly, the photolysis of 50 μM 2NB in the reactor was monitored by determining its concentration every 5 min for a total of 35 min, during which 2NB was almost completely decayed. The concentration of 2NB was measured using UHPLC-PDA, and the settings (e.g., column, mobile phase, gradient, oven temperature) were the same as those for VL decay analysis (Text S3). The channel with UV absorption at 254 nm was used for the quantification of 2NB. The concentration of 2NB in the reactor followed exponential decay, and its decay rate constant was determined using the following equation:

$$\ln\left(\frac{[2\text{NB}]_t}{[2\text{NB}]_0}\right) = -j(2\text{NB}) \times t \quad (\text{Eq. S4})$$

where $[2\text{NB}]_t$ and $[2\text{NB}]_0$ are the 2NB concentrations at time t and 0, respectively. The calculated 2NB decay rate constant, $j(2\text{NB})$, was 0.0026 s^{-1} . The following equation can also be used to calculate $j(2\text{NB})$:

$$j(2\text{NB}) = 2.303 \times (10^3 \text{ cm}^3 \text{ L}^{-1} \times 1 \text{ mol}/N_A \text{ mlc}) \times \sum \left(I'_\lambda \times \Delta\lambda \times \varepsilon_{2\text{NB},\lambda} \times \Phi_{2\text{NB}} \right) \quad (\text{Eq. S5})$$

where N_A is Avogadro's number, I'_λ is the actinic flux ($\text{photons cm}^{-2} \text{ s}^{-1} \text{ nm}^{-1}$), $\Delta\lambda$ is the wavelength interval between actinic flux data points (nm), and $\varepsilon_{2NB,\lambda}$ and $\Phi_{2NB,\lambda}$ are the base-10 molar absorptivity ($\text{M}^{-1} \text{ cm}^{-1}$) and quantum yield ($\text{molecule photon}^{-1}$) for 2NB, respectively. Values of $\varepsilon_{2NB,\lambda}$ (in water) at each wavelength under 298 K and a wavelength-independent Φ_{2NB} value of 0.41 were adapted from Galbavy et al. (2010). Finally, I'_λ was estimated through Eq. S5. The estimated photon flux in the aqueous reactor is shown in Figure S2.

The actinic flux during a haze event over Beijing (40° N , 116° E) on January 12, 2013, at 12:00 pm (GMT+8) (Che et al., 2014) estimated using the National Center for Atmospheric Research Tropospheric Ultraviolet-Visible (TUV) Radiation Model (http://cprm.acom.ucar.edu/Models/TUV/Interactive_TUV/) is also shown in Figure S2. The parameters used for the Quick TUV calculator were: Overhead Ozone Column: 300 du; Surface Albedo: 0.1; Ground Elevation: 0 km asl; Measured Altitude: 0 km asl; Clouds optical depth: 0, base: 4, top: 5; Aerosols optical depth: 2.5, single scattering albedo: 0.9, Angstrom exponent: 1; Sunlight direct beam, diffuse down, diffuse up: 1; 4 streams transfer model. For clear days, the actinic flux was estimated over Beijing (at the same date and time) using the default parameters.

Table S1. Typical fragmentation behavior observed in MS/MS spectra for individual functional groups from Holčápek et al. (2010).

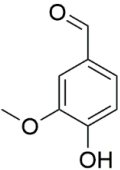
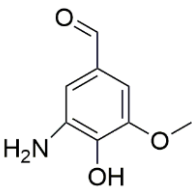
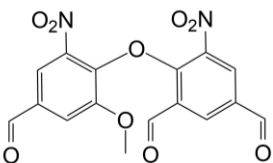
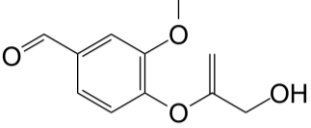
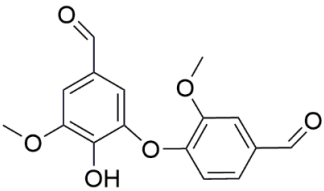
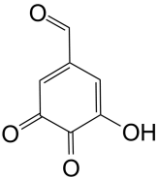
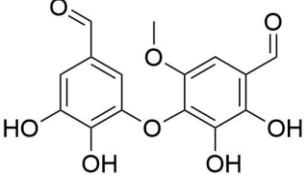
Functional group	Fragment ions	MS/MS loss
Nitro (RNO ₂)	[M+H-OH] ⁺ *	-OH
	[M+H-H ₂ O] ⁺	-H ₂ O
	[M+H-NO] ⁺ *	-NO
	[M+H-NO ₂] ⁺ *	-NO ₂
Nitroso (RNO)	[M+H-NO] ⁺	-NO
Carboxylic acid (ROOH)	[M+H-H ₂ O] ⁺	-H ₂ O
	[M+H-CO ₂] ⁺	-CO ₂
	[M+H-H ₂ O-CO] ⁺	-H ₂ O-CO
Phenol (ROH)	[M+H-H ₂ O] ⁺	-H ₂ O
	[M+H-CO] ⁺	-CO
Methoxy (ROCH ₃)	[M+H-CH ₃] ⁺ *	-CH ₃
	[M+H-CH ₃ O] ⁺ *	-CH ₃ O
	[M+H-CH ₃ OH] ⁺	-CH ₃ OH
	[M+H-HCOH] ⁺	-HCOH
Ester (R ¹ COOR ²)	[M+H-R ² OH] ⁺	-R ² OH
	[M+H-R ² OH-CO] ⁺	-R ² OH-CO
Amine	[M+H-NH ₃] ⁺	-NH ₃
Aldehyde (RCHO)	[M+H-CO] ⁺	-CO

Table S2. Reaction conditions, initial VL (and GUA) decay rates, normalized abundance of products, and average carbon oxidation state (<OS_c>) in each experiment. Except where noted, the reaction systems consisted of VL (0.1 mM); GUA (0.1 mM), AN (1 mM); sodium nitrate (SN) (1 mM); VOC (IPA) (1 mM) or inorganic anions (NaBC) (1 mM) under air-saturated conditions after 6 h of simulated sunlight irradiation. Analyses were performed using UHPLC-qToF-MS equipped with an ESI source and operated in the positive ion mode.

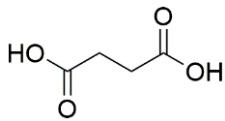
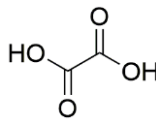
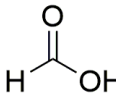
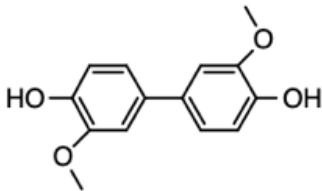
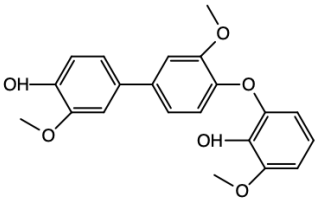
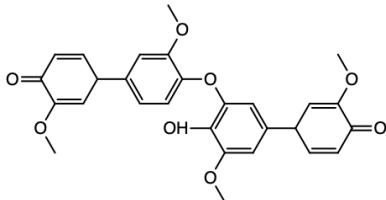
Exp no.	pH	Reaction conditions	Initial VL (and GUA) decay rates (min ⁻¹) ^b	Ratio of 50 most abundant products to total products ^c	Normalized abundance of products ^d	Normalized abundance of N-containing compounds ^d	<OS _c > ^e
A1	2.5	VL*	2.8×10^{-3}	0.59	1.7	-	-0.05
A2		VL+AN	2.5×10^{-3}	0.63	1.4	5.3×10^{-2}	-0.04
A3		VL*	2.1×10^{-3}	0.53	1.9	--	-0.04
A4	3	VL+AN	2.1×10^{-3}	0.56	1.9	3.6×10^{-2}	-0.05
A5	4	VL*	1.9×10^{-3}	0.58	0.26	--	-0.16
A6		VL* (N ₂ -saturated)	4.6×10^{-4}	0.96	4.7×10^{-2}	--	-0.24
A7		VL+AN	1.9×10^{-3}	0.53	0.37	1.7×10^{-2}	-0.13
A8		VL+AN (N ₂ -saturated)	2.9×10^{-4}	0.89	0.12	6.3×10^{-3}	-0.21
A9		VL*+IPA	1.6×10^{-3}	0.58	0.63	--	-0.10
A10		VL*+NaBC	2.3×10^{-3}	0.45	0.37	--	-0.11
A11		VL+AN+IPA	1.9×10^{-3}	0.52	1.4	1.7×10^{-2}	0.08
A12		VL+AN+NaBC	1.9×10^{-3}	0.53	1.6	1.6×10^{-2}	0.08
A13		VL+SN	--	0.51	0.42	1.7×10^{-2}	-0.07
A14		VL* (0.01 mM) ^a	--	0.90	0.37	--	-0.07
A15		VL (0.01 mM) + AN (0.01 mM)	--	0.77	0.40	8.6×10^{-3}	0.12
A16		VL (0.01 mM) + AN	--	0.42	0.45	1.2×10^{-2}	-0.06
A17		GUA only	9.0×10^{-4}	0.77	--	--	-0.28
A18		GUA+VL	GUA: 2.0×10^{-3} VL: 6.2×10^{-4}	0.60	2.2	--	-0.27
A19		GUA+AN	1.1×10^{-3}	0.77	--	--	-0.26

^aIrradiation time for VL* (0.01 mM, A14) was 3 h. ^bThe data fitting was performed in the initial linear region. ^cRatio of the normalized abundance of the 50 most abundant products to that of total products, except for direct GUA photodegradation (A17), GUA+VL (A18), and GUA+AN (A19) whose ratios are based on the absolute signal area of products. ^dThe normalized abundance of products was calculated using Eq. 2. ^e<OS_c> of the 50 most abundant products.

Table S3. Examples of proposed molecular structures for products identified from vanillin (and guaiacol) photo-oxidation experiments in this study.

No.	Formula	DBE	Proposed structure	MS/MS fragment ions		
1	C ₈ H ₈ O ₃	5		-CO-CH ₃ OH	-CO	-CO-CH ₃ OH-CO
2	C ₈ H ₉ NO ₃	5		-CO-CH ₃	-NH ₃	
3	C ₁₆ H ₁₀ N ₂ O ₉	13		-NO ₂		
4	C ₁₀ H ₁₀ O ₅	6		-CH ₃ OH	-CH ₃ OH-CO	
5	C ₁₆ H ₁₄ O ₆	10		-CO-CH ₃ OH-CO	-CO-CH ₃ OH-CO-CH ₃ OH	-CO-CH ₃ OH-CO-CO
6	C ₇ H ₄ O ₄	6		-CO	-CO-CO	
7	C ₁₅ H ₁₂ O ₈	10		-CO	-CH ₃	

8	$C_8H_6O_4$	6		-CO	-CO-CO	
9	$C_{15}H_{12}O_8$	10		-COOH		
10	$C_5H_5N_3O_2$	5		-NH		
11	$C_7H_4N_2O_7$	7				
12	$C_{15}H_{14}O_8$	9		-CO-CH3OH- CO-CO	-CO- CH3OH- CO-H2O	-CO- CH3OH-CO
13	$C_8H_8O_4$	5		-CO-CH3OH	-CO	-H2O
14	$C_8H_8O_5$	5		-CO-CH3OH	-CO2	-CH3OH
15	$C_{23}H_{18}O_9$	15				

16	$C_4H_6O_4$	2		From IC analysis
17	$C_2H_2O_4$	2		
18	CH_2O_2	1		
19	$C_{14}H_{14}O_4$	8		
20	$C_{21}H_{20}O_6$	12		
21	$C_{28}H_{24}O_8$	17		

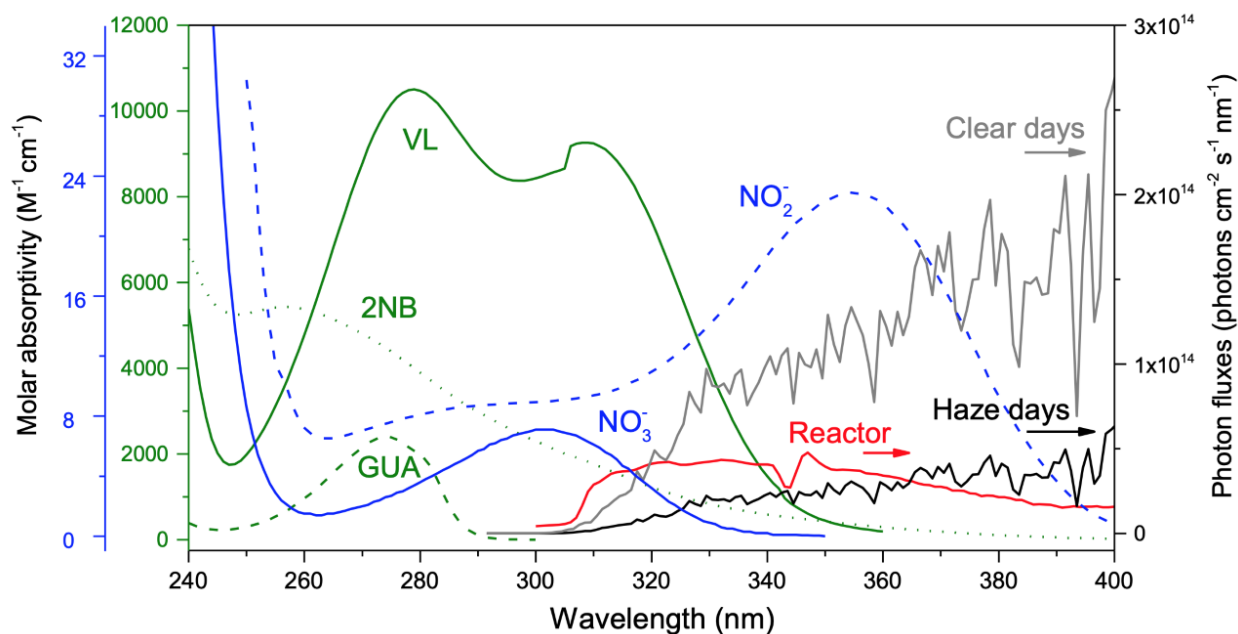


Figure S1. The base-10 molar absorptivities (ϵ , $\text{M}^{-1} \text{cm}^{-1}$) of vanillin (VL, green solid line), 2-nitrobenzaldehyde (2NB, green dotted line), guaiacol (GUA, green dashed line), NO_2^- (blue dashed line), NO_3^- (blue solid line), and photon flux in the aqueous reactor (red line) during typical haze days (black line) or clear days (grey line) in Beijing, China. The ϵ values for 2NB and NO_2^- were adapted from Galbavy et al. (2010) and Chu and Anastasio (2007), respectively.

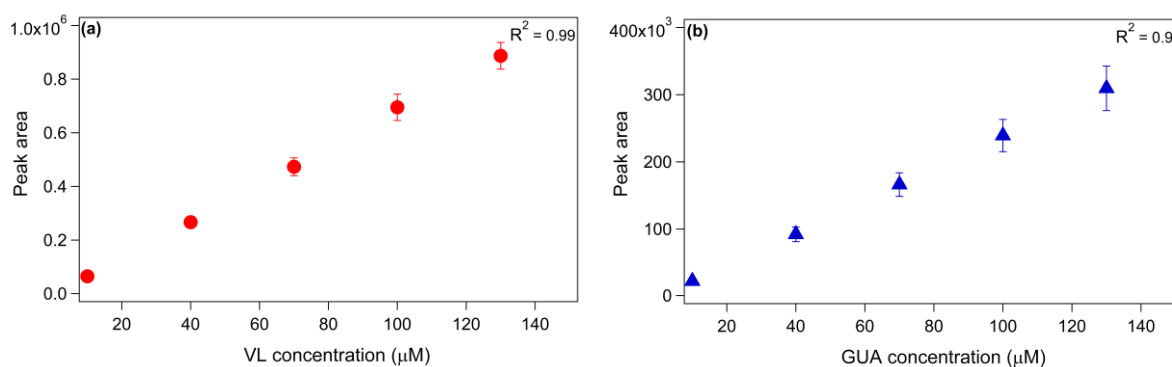


Figure S2. Calibration curves for (a) VL and (b) GUA standard solutions (10-130 μM).

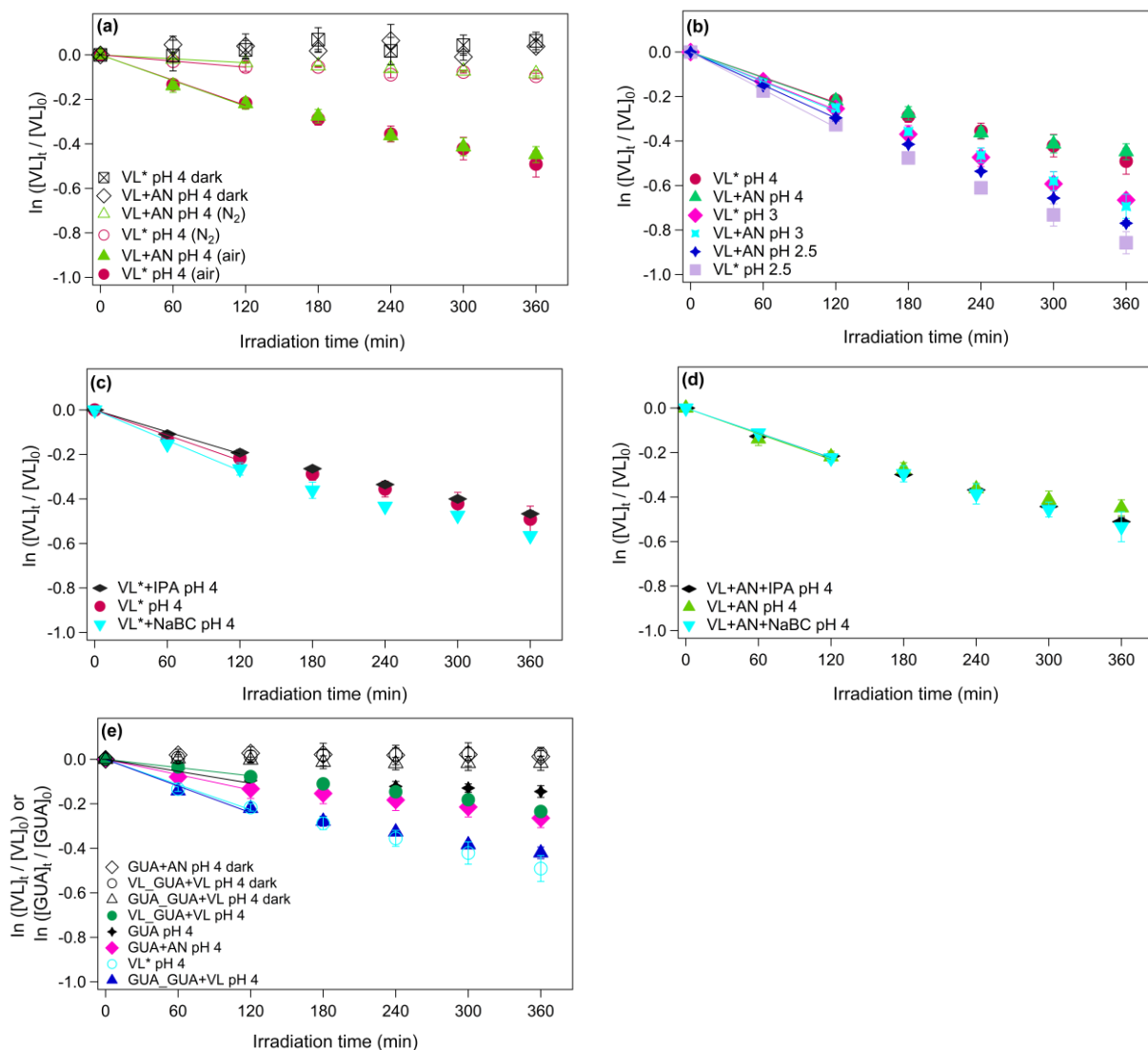


Figure S3. (a-d) The decay of VL under different experimental conditions for direct photosensitized oxidation of VL (VL*) and nitrate-mediated VL photo-oxidation (VL+AN): (a) Effect of secondary oxidants from VL triplets on VL* and VL+AN at pH 4 under N_2 - (A6, A8) and air-saturated (A5, A7) conditions. (b) Effect of pH on VL* and VL+AN at pH 2.5 (A1, A2), 3 (A3, A4), and 4 (A5, A7) under air-saturated conditions. (c) Effect of the presence of VOCs and inorganic anions: IPA (A9) and NaBC (A10) on VL* at pH 4 under air-saturated conditions. (d) Effect of the presence of VOCs and inorganic anions: IPA (A11) and NaBC (A12) on VL+AN at pH 4 under air-saturated conditions. (e) The decay of VL (and GUA) during direct GUA photodegradation (A17) and photo-oxidation of GUA in the presence of VL (GUA+VL; A18) or nitrate (GUA+AN; A19) at pH 4 under air-saturated conditions after 6 h of simulated sunlight irradiation. Error bars represent 1 standard deviation.

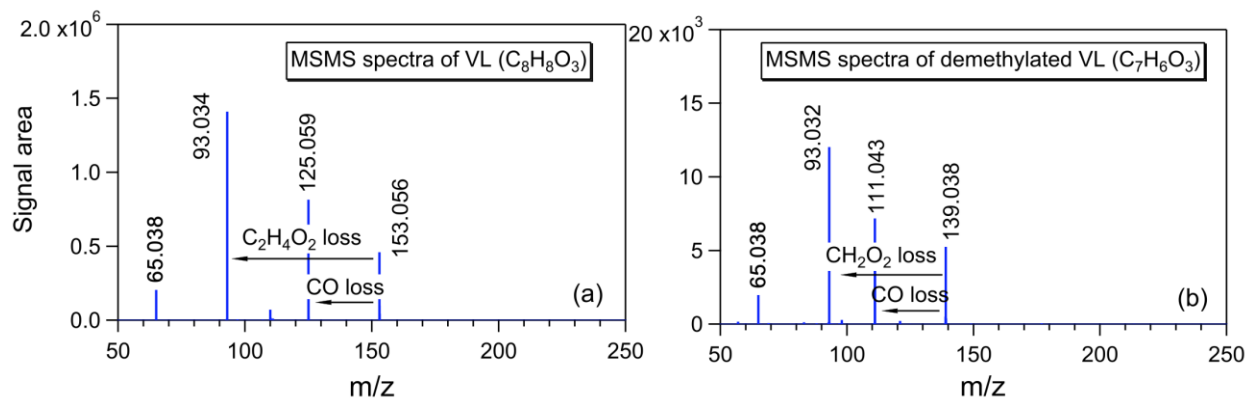


Figure S4. MS/MS spectra of (a) VL and (b) demethylated VL. The arrows indicate possible fragmentation pathways of VL and demethylated VL.

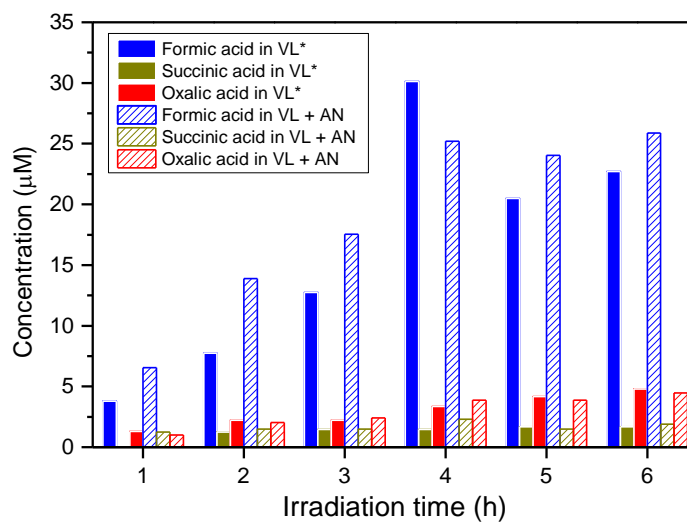


Figure S5. The concentration of formic, oxalic, and succinic acid at different reaction times for VL* (A5) and VL+AN (A7) at pH 4 under air-saturated conditions.

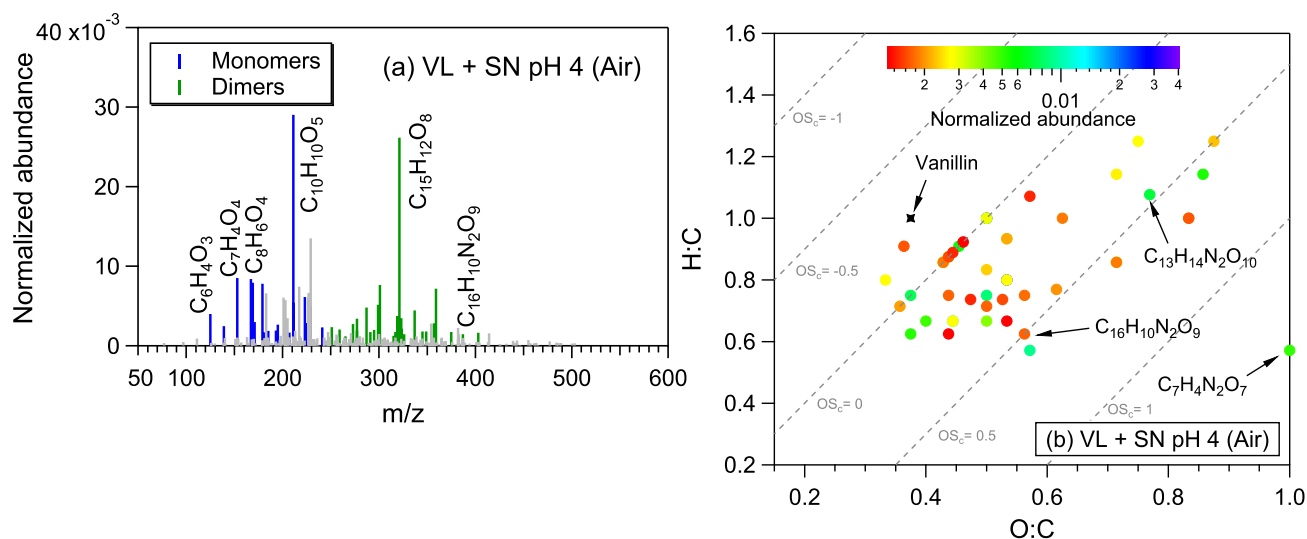


Figure S6. (a) Reconstructed mass spectra of assigned peaks and (b) van Krevelen diagram of the 50 most abundant products from VL+SN (A13) at pH 4 under air-saturated conditions after 6 h of simulated sunlight irradiation. The normalized abundance of products was calculated from the ratio of the peak area of the product to that of VL (Eq. 2). The 50 most abundant products contributed more than half of the total normalized abundance of products, and they were identified as monomers (blue) and dimers (green). Grey peaks denote peaks with low abundance or unassigned formula. Examples of high-intensity peaks were labeled with the corresponding neutral formulas. The color bar denotes the normalized abundance of products. The grey dashed lines indicate the carbon oxidation state values (e.g., OS_c = -1, 0, and 1).

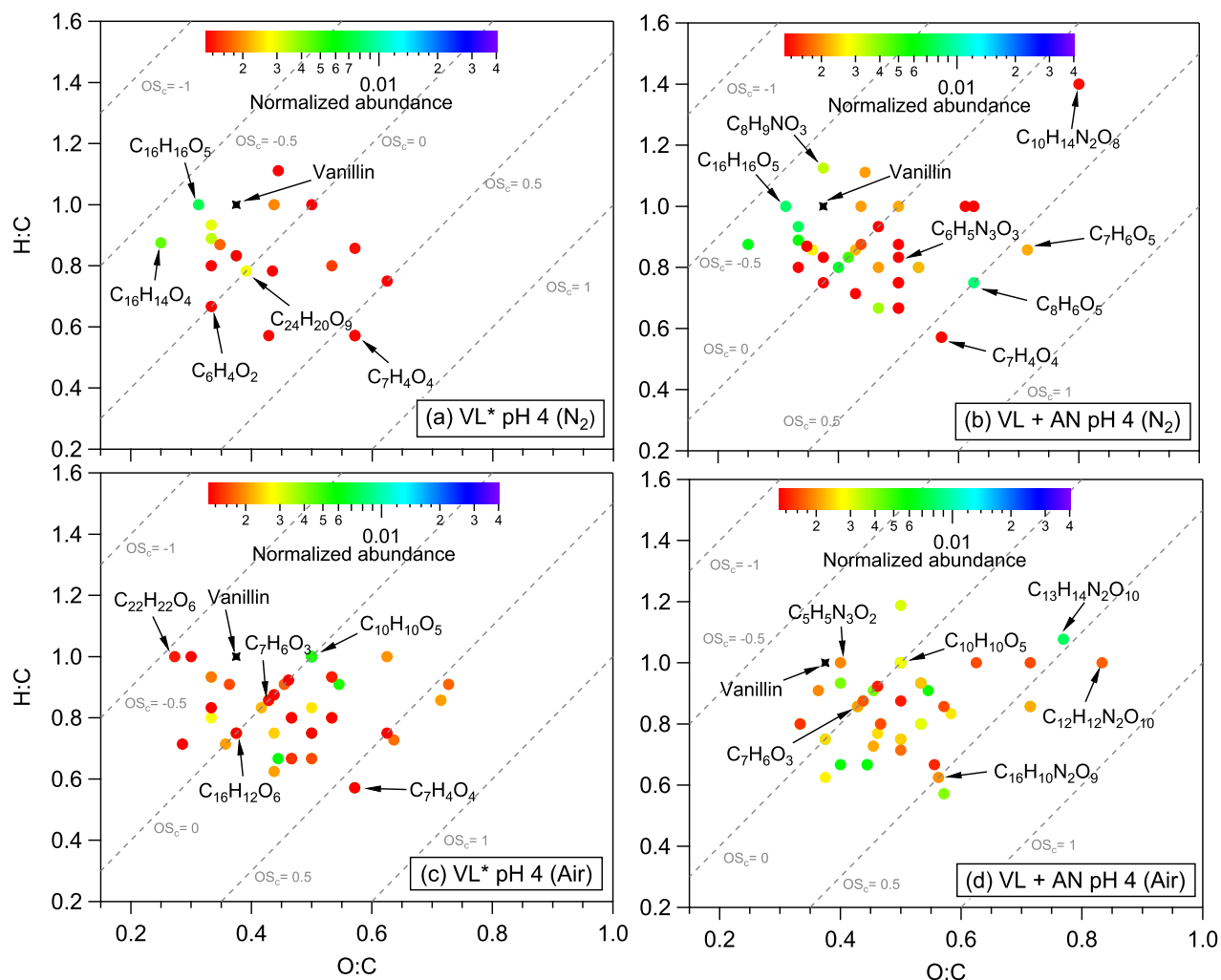


Figure S7. van Krevelen diagrams of the 50 most abundant products from (a) VL* (N_2 -saturated; A6), (b) VL+AN (N_2 -saturated; A8), (c) VL* (air-saturated; A5), and (d) VL+AN (air-saturated; A7) at pH 4 after 6 h of simulated sunlight irradiation. The color bar denotes the normalized abundance of products. The grey dashed lines indicate the carbon oxidation state values (e.g., $OS_c = -1, 0, \text{and } 1$).

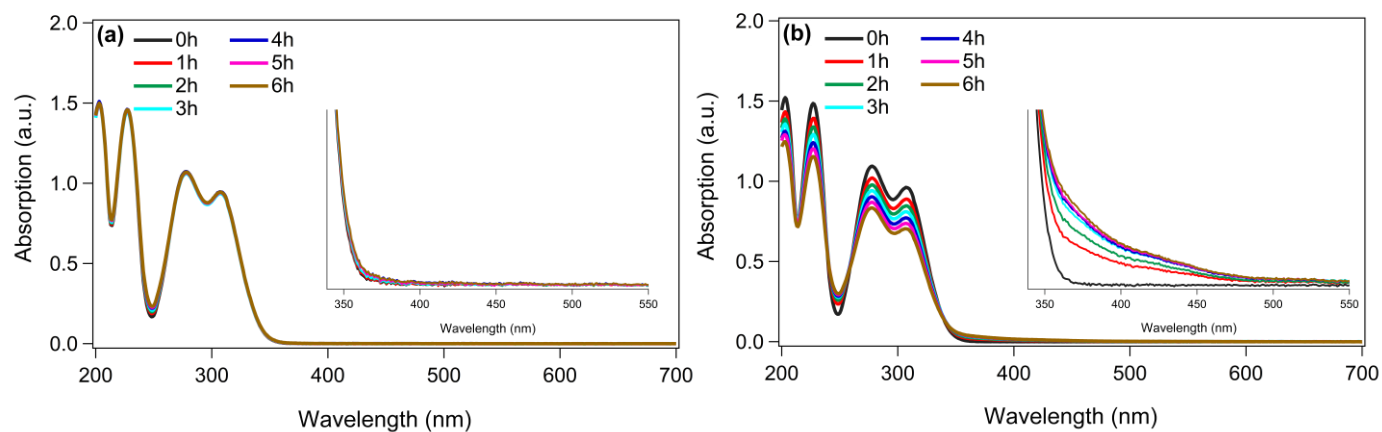


Figure S8. UV–Vis absorption spectra of VL* (A6, A5; pH 4) under (a) N₂- and (b) air-saturated conditions at different time intervals. The insets show the absorbance enhancement from 350 to 550 nm.

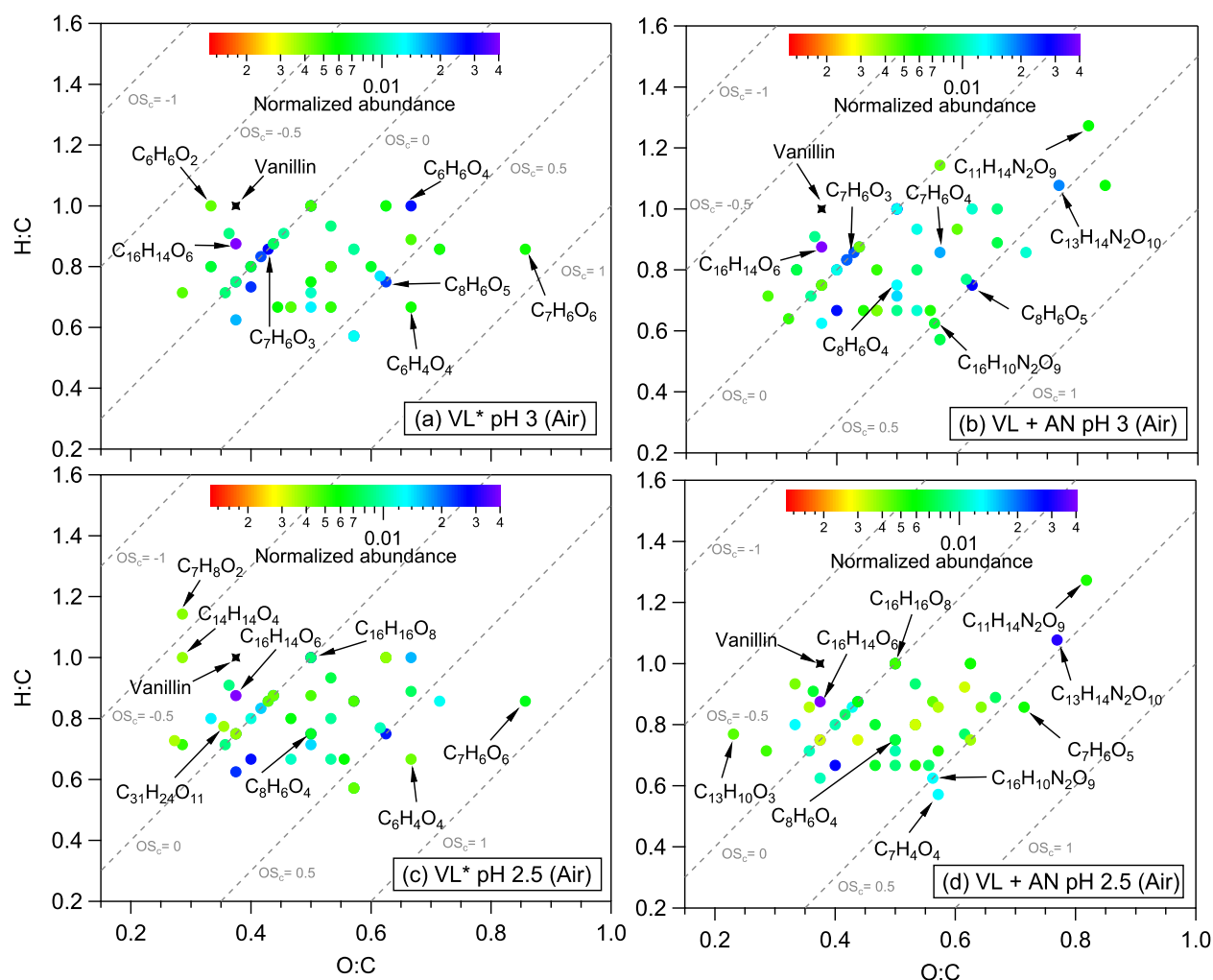


Figure S9. van Krevelen diagrams of the 50 most abundant products from (a) VL* pH 3 (A3), (b) VL+AN pH 3 (A4), (c) VL* pH 2.5 (A1), and (d) VL+AN pH 2.5 (A2) under air-saturated conditions after 6 h of simulated sunlight irradiation. The color bar denotes the normalized abundance of products. The grey dashed lines indicate the carbon oxidation state values (e.g., OS_c = -1, 0, and 1).

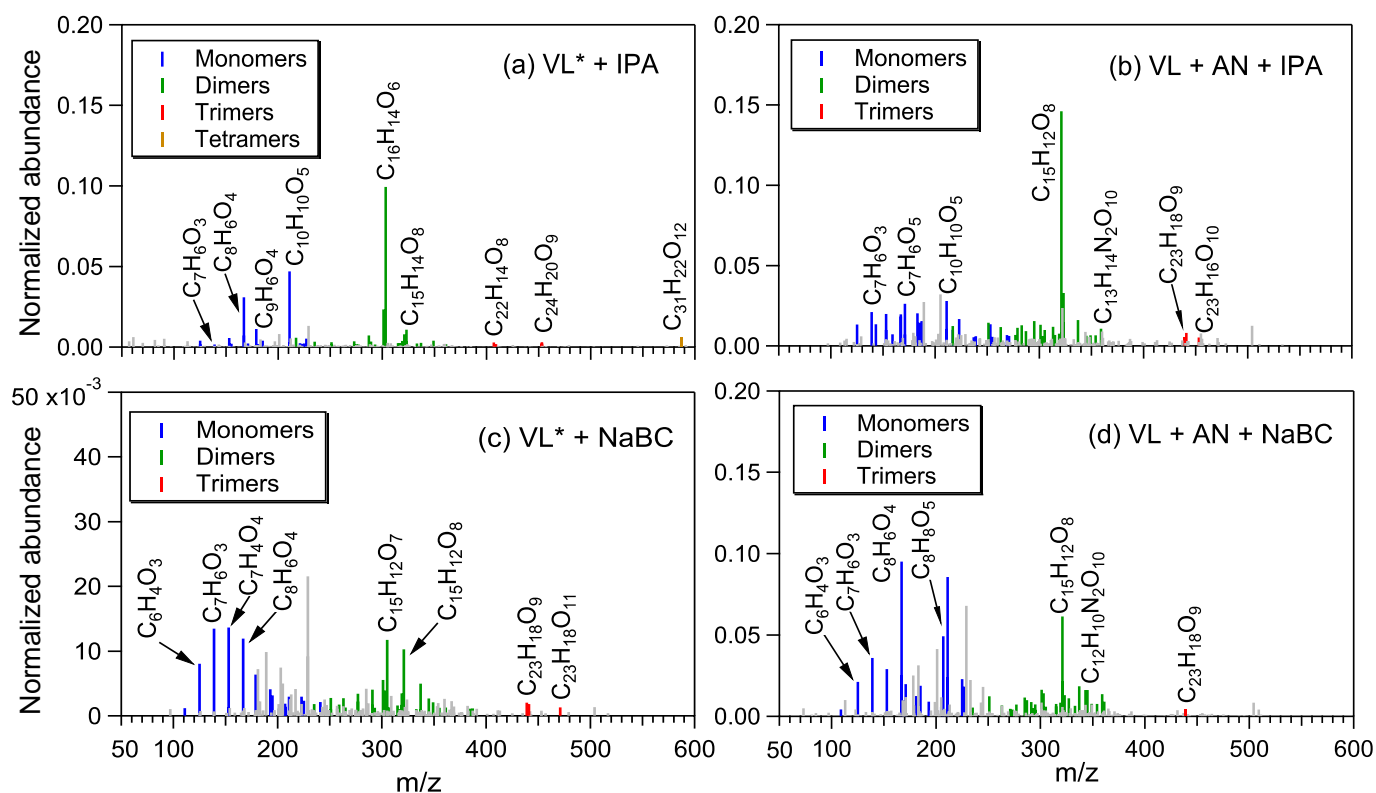


Figure S10. Reconstructed mass spectra of assigned peaks from (a) VL*+IPA (A9), (b) VL+AN+IPA (A11), (c) VL*+NaBC (A10), and (d) VL+AN+NaBC (A12) at pH 4 under air-saturated conditions after 6 h of simulated sunlight irradiation. The normalized abundance of products was calculated from the ratio of the peak area of the product to that of VL (Eq. 2). The 50 most abundant products contributed more than half of the total normalized abundance of products, and they were identified as monomers (blue), dimers (green), trimers (red), and tetramers (orange). Grey peaks denote peaks with low abundance or unassigned formula. Examples of high-intensity peaks were labeled with the corresponding neutral formulas. Note the different scales on the y-axes.

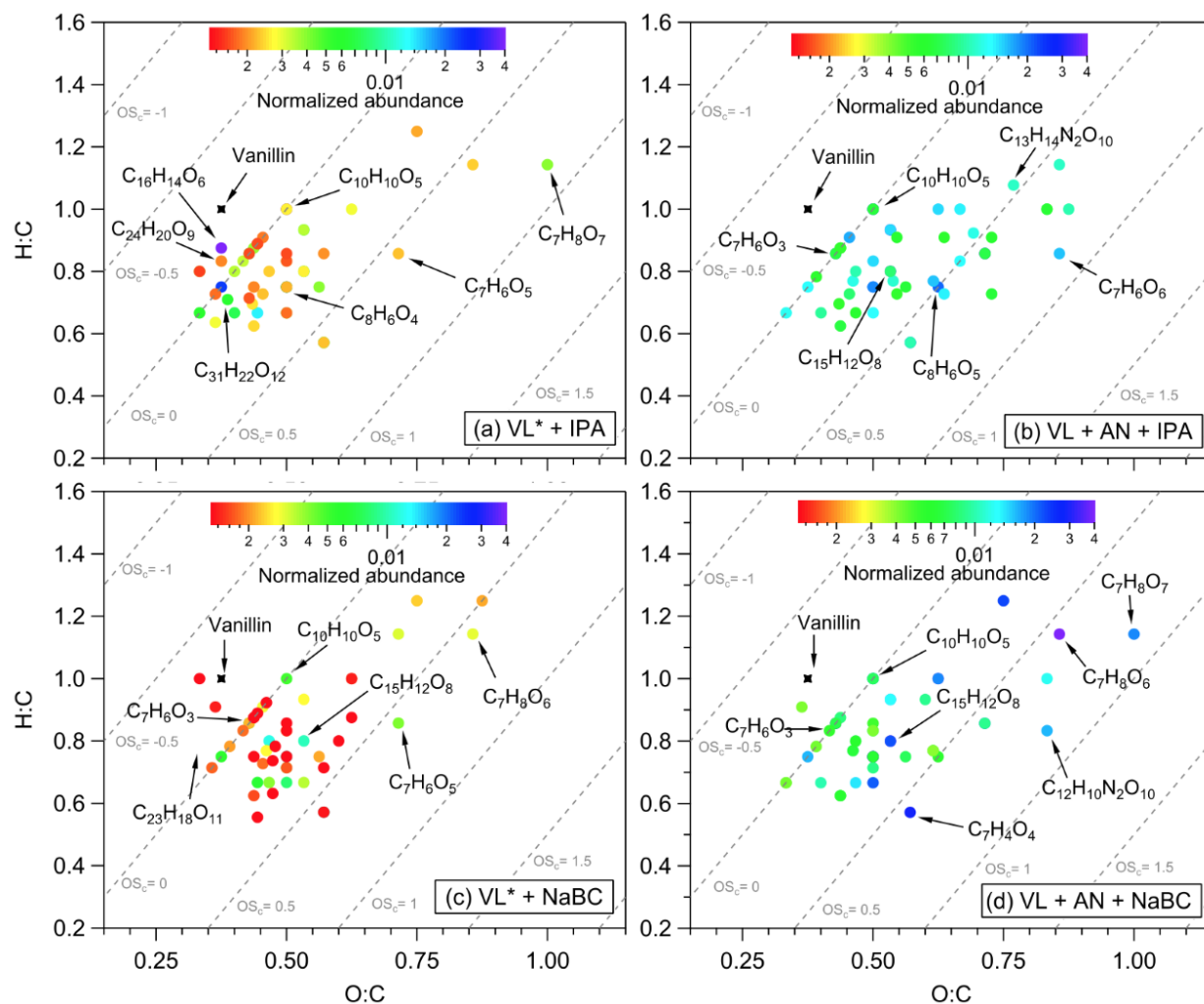


Figure S11. van Krevelen diagrams of the 50 most abundant products from (a) VL*+IPA (A9), (b) VL+AN+IPA (A11), (c) VL*+NaBC (A10), and (d) VL+AN+NaBC (A12) at pH 4 under air-saturated conditions after 6 h of simulated sunlight irradiation. The color bar denotes the normalized abundance of products. The grey dashed lines indicate the carbon oxidation state values (e.g., OS_c = -1, 0, and 1).

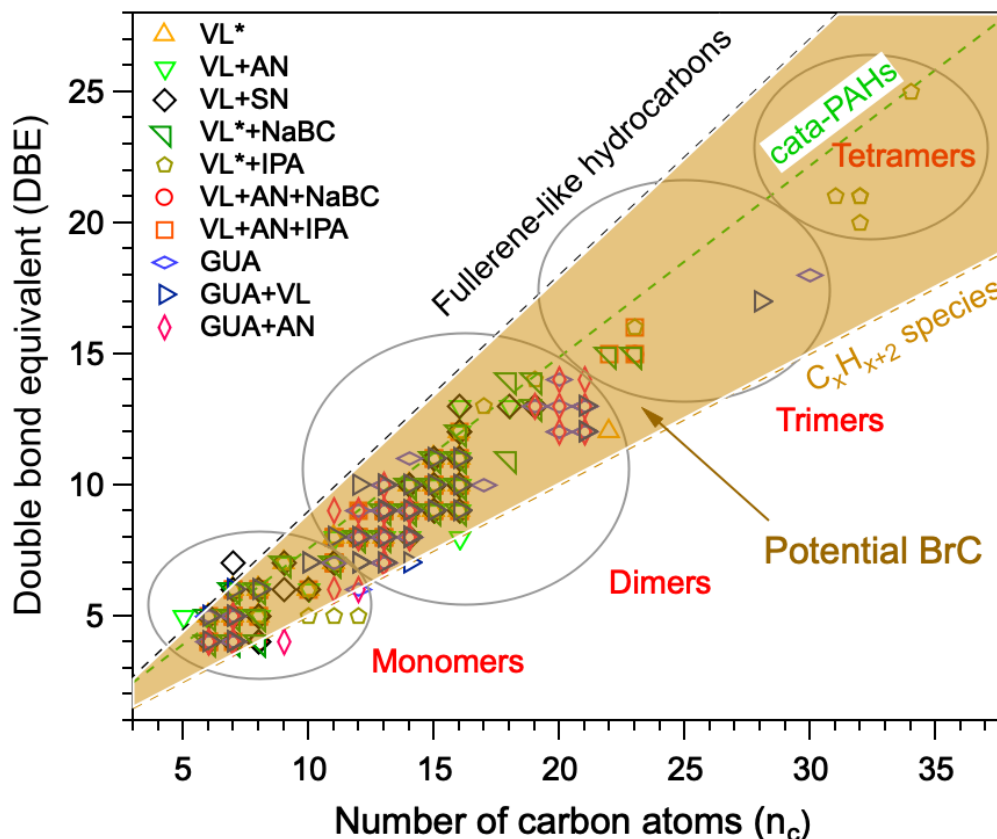


Figure S12. The plot of the double bond equivalent (DBE) values vs. number of carbon atoms (n_c) (Lin et al., 2018) for the 50 most abundant products from pH 4 experiments under air-saturated conditions. Dashed lines indicate DBE reference values of fullerene-like hydrocarbons (Lobodin et al., 2012) (black dashed line), cata-condensed polycyclic aromatic hydrocarbons (PAHs) (Siegmann and Sattler, 2000) (green dashed line), and linear conjugated polyenes (general formula C_xH_{x+2}) (brown dashed line). Data points within the shaded area are potential BrC chromophores. Light grey circles show the classification of the data points as monomers, dimers, trimers, or tetramers.

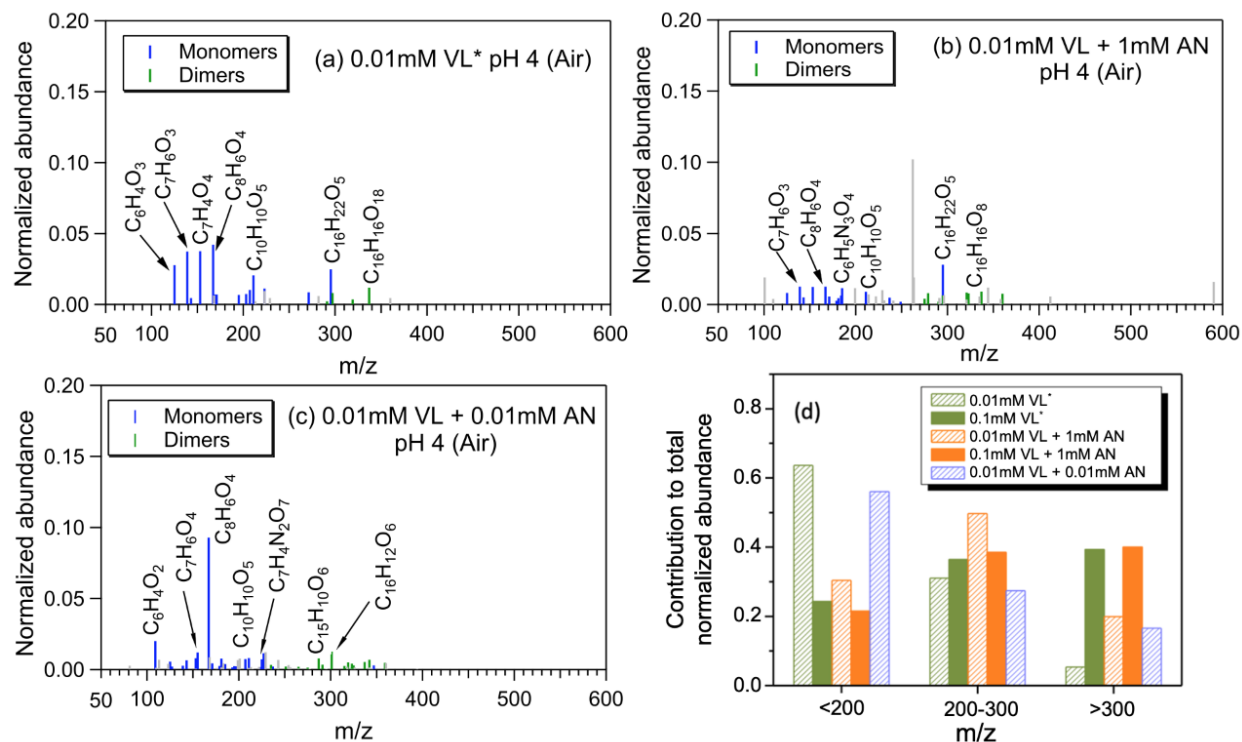


Figure S13. Reconstructed mass spectra of assigned peaks from (a) 0.01 mM VL* (A14), (b) 0.01 mM VL + 1 mM AN (A16), and (c) 0.01 mM VL + 0.01 mM AN (A15) at pH 4 under air-saturated conditions after 6 h of simulated sunlight irradiation. The normalized abundance of products was calculated from the ratio of the peak area of the product to that of VL (Eq. 2). The 50 most abundant products contributed more than half of the total normalized abundance of products, and they were identified as monomers (blue) and dimers (green). Grey peaks denote peaks with low abundance or unassigned formula. Examples of high-intensity peaks were labeled with the corresponding neutral formulas. (d) Contributions of different m/z ranges to the normalized abundance of products from experiments with low [VL] = 0.01 mM (A14-A16) and high [VL] = 0.1 mM (A5 and A7) at pH 4 under air-saturated conditions after 6 h of simulated sunlight irradiation.

References

- Bateman, A. P., Laskin, J., Laskin, A., and Nizkorodov, S. A.: Applications of high-resolution electrospray ionization mass spectrometry to measurements of average oxygen to carbon ratios in secondary organic aerosols, *Environ. Sci. Technol.*, 46, 8315–8324, <https://doi.org/10.1021/es3017254>, 2012.
- Che, H., Xia, X., Zhu, J., Li, Z., Dubovik, O., Holben, B., Goloub, P., Chen, H., Estelles, V., Cuevas-Agulló, E., Blarel, L., Wang, H., Zhao, H., Zhang, X., Wang, Y., Sun, J., Tao, R., Zhang, X., and Shi, G.: Column aerosol optical properties and aerosol radiative forcing during a serious haze-fog month over North China Plain in 2013 based on ground-based sunphotometer measurements, *Atmos. Chem. Phys.*, 14, 2125–2138, <https://doi.org/10.5194/acp-14-2125-2014>, 2014.
- Chu, L. and Anastasio, C.: Temperature and wavelength dependence of nitrite photolysis in frozen and aqueous solutions, *Environ. Sci. Technol.*, 41, 3626–3632, <https://doi.org/10.1021/es062731q>, 2007.
- Erngren, I., Haglöf, J., Engskog, M. K. R., Nestor, M., Hedeland, M., Arvidsson, T., and Pettersson, C.: Adduct formation in electrospray ionisation-mass spectrometry with hydrophilic interaction liquid chromatography is strongly affected by the inorganic ion concentration of the samples, *J. Chromatogr. A*, 1600, 174–182, <https://doi.org/10.1016/j.chroma.2019.04.049>, 2019.
- Galbavy, E. S., Ram, K., and Anastasio, C.: 2-Nitrobenzaldehyde as a chemical actinometer for solution and ice photochemistry, *J. Photochem. Photobiol. A*, 209, 186–192, <https://doi.org/10.1016/j.jphotochem.2009.11.013>, 2010.
- Holčapek, M., Jirásko, R., and Líba, M.: Basic rules for the interpretation of atmospheric pressure ionization mass spectra of small molecules, *J. Chromatogr. A*, 1217, 3908–3921, <https://doi.org/10.1016/j.chroma.2010.02.049>, 2010.
- Koch, B. P. and Dittmar, T.: From mass to structure: an aromaticity index for high-resolution mass data of natural organic matter, *Rapid Commun. Mass Spectrom.*, 20, 926–932, <https://doi.org/10.1002/rcm.7433>, 2006.
- Lin, P., Fleming, L. T., Nizkorodov, S. A., Laskin, J., and Laskin, A.: Comprehensive molecular characterization of atmospheric brown carbon by high resolution mass spectrometry with electrospray and atmospheric pressure photoionization, *Anal. Chem.*, 90, 12493–12502, <https://doi.org/10.1021/acs.analchem.8b02177>, 2018.
- Lobodin, V. V., Marshall, A. G., and Hsu, C. S.: Compositional space boundaries for organic compounds, *Anal. Chem.*, 84, 3410–3416, <https://doi.org/10.1021/ac300244f>, 2012.
- Roemmelt, A. T., Steuer, A. E., and Kraemer, T.: Liquid chromatography, in combination with quadrupole time-of-flight instrument, with sequential window acquisition of all theoretical fragment-ion spectra acquisition: validated quantification of 39 antidepressants in whole blood

as part of a simultaneous screening and quantification procedure, *Anal. Chem.*, 87, 9294–9301, <https://doi.org/10.1021/acs.analchem.5b02031>, 2015.

Siegmann, K. and Sattler, K. D.: Formation mechanism for polycyclic aromatic hydrocarbons in methane flames, *J. Chem. Phys.*, 112, 698–709, <https://doi.org/10.1063/1.480648>, 2000.

Zhou, W., Mekic, M., Liu, J., Loisel, G., Jin, B., Vione, D., and Gligorovski, S.: Ionic strength effects on the photochemical degradation of acetosyringone in atmospheric deliquescent aerosol particles, *Atmos. Environ.*, 198, 83–88, <https://doi.org/10.1016/j.atmosenv.2018.10.047>, 2019.